Optimization of a novel cryogenic CO_2 capture process by response surface methodology (RSM)

Chunfeng Song [1, *], Yutaka Kitamura [2], Shuhong Li [2]

[1] *Collaborative Research Center for Energy Engineering, Institute of Industrial Science, The University of Tokyo, 4-6-1 Komaba, Meguro-Ku, Tokyo 153-8505, Japan*

[2] *Graduate School of Life and Environmental Sciences, University of Tsukuba, 1-1-1, Tennodai, Tsukuba, Ibaraki 305-8572, Japan*

* Corresponding author. Tel.: +81 0298-53-4655; Fax: +81 0298-53-4655.

E-mail address: songcf@iis.u-tokyo.ac.jp

Abstracts

CO_2 capture and storage (CCS) technologies play a significant role in greenhouse gas (GHG) control. In our previous work, a novel cryogenic CO_2 capture process based on free piston Stirling coolers (FPSCs) was developed. In order to improve capture efficiency, the exploited system was optimized using response surface methodology (RSM). The influence of capture conditions on performance was investigated based on three levels and variables and in central composite design (CCD). The parameters contain flow rate (X_1: 1 ~ 3 L/min), temperature of FPSC-1 (X_2: -30 ~ -10 °C) and idle operating time (X_3: 3 ~ 5 h). The objective of this work is to ascertain the optimal performance of the system (with maximum CO_2 recovery, CO_2 productivity and minimum energy consumption). The experimental data was fitted to a second-order polynomial equation using multiple regression analysis and analyzed using analysis of variance (ANOVA). The dimensional response surface plots and the contour plots derived from the mathematical models were utilized to determine optimum conditions. Results indicate the optimum conditions were: flow rate of 2.16 L/min, temperature of FPSC-1 of -18 °C and operating time of 3.9 h. Under these conditions, the whole process can capture 95.20 % CO_2 with 0.52 MJ/kg $_{\text{captured}}$ CO_2 input electricity. Meanwhile, the CO_2 productivity is 44.37 kg CO_2/h.

Keywords: Cryogenic, CO_2 capture, response surface methodology, CO_2 recovery, energy consumption, CO_2 productivity

Nomenclature

X1	Flow rate of flue gas, L/min
X2	Temperature of FPSC-1, °C
X3	Idle operating time, h
η	CO_2 recovery
φ	CO_2 productivity
Abbreviations	
ANOVA	Analysis of variance
CCD	Central composite design
CCS	CO_2 capture and storage
CFZ	Controlled freeze zone
EC	Energy consumption
FPSC	Free piston Stirling cooler
GHG	Greenhouse gas
RSM	Response surface methodology
TPSA	Temperature pressure swing adsorption

1. Introduction

Climate issues have attracted more and more attention in recent decades. It is known that greenhouse gas (GHG) is one of the most important influences on climate change [1]. The major species of GHG include methane (CH_4), carbon dioxide (CO_2), nitrous oxide (N_2O) and fluorinated gases (HFCs, PFCs and SF_6) [2]. Of these, CO_2 contributes about 70 % to the enhanced greenhouse effect and global warming, and therefore needs primary mitigation [3]. The emission of CO_2 is accompanied by the burning of fossil fuel from large fixed industrial stations (*i.e.* coal-fired power plants, steel and cement plants *etc.*). At present, the main post combustion CO_2 capture technologies include: absorption, adsorption, membrane separation and cryogenic fractionation [4]. Although current commercial technologies such as amine based scrubbing are available for CO_2 capture from flue gas, the capital and operating cost of capture is still too high [5-8]. This has become a major barrier for the application of CO_2 capture in power plant sectors and other CO_2 emitters. Therefore, more research is required to improve CO_2 capture efficiency and reduce capture costs [9,10].

As an alternative to existing methods, cryogenic separation technologies have also attracted attention in recent decades. Holmes and Ryan (1982) developed a cryogenic distillative process to separate acid gases (mainly CO_2) from methane [11]. Thomas and Denton (1988) proposed a controlled freeze zone (CFZ) process to treat high CO_2/N_2 content natural gas, and the process combined two low temperature distillation and a CO_2 solidification units [12]. Clodic and Younes (2002) built an

anti-sublimation CO_2 capture process named AnSU® [13]. In their process, the flue gas was first chilled to the CO_2 freezing point and then the CO_2 in the gas stream frosted on the cold surface of the heat exchanger. Tuinier *et al*. (2011, 2012) exploited a cryogenic packed bed to recover CO_2 from the flue gas and purify the biogas [14,15]. During the process, H_2O and CO_2 can be separated from the different locations in the bed by the difference in freezing point. Berstad *et al*. (2012) put forward a low temperature distillation process to remove CO_2 from natural gas [16]. The CO_2 concentration of the natural gas was reduced from an initial 50.6% to 50 ppm by three distillation columns, and the purity of the final CO_2 product is 94.35%. It should be noted that the intricate phase variation (liquefaction or solidification) and thermodynamic process (mass and heat transfer) usually accompany with the designed cryogen capture processes [17]. In order to improve capture efficiency and minimize energy consumption, a good understanding of the complex relationships among the operation parameters involved in the cryogenic CO_2 capture processes is necessary.

In light of these concerns, an effective approach that reveals the effect of key process parameters and their interactions on CO_2 capture performance is particularly significant. Response surface methodology (RSM) is a statistical technique for optimizing complex processes due to its more efficient and easier arrangement of experiments [18]. This method is less laborious and time-consuming than other approaches applied to optimize a process. Although a reduced number of experimental trials are needed to evaluate multiple factors and their interactions, they are helpful to determine the target value. Hence, RSM provides an effective tool for

investigating aspects that affect the desired response if there are many factors and interactions in the experiment. To optimize the process, RSM can be employed to determine a suitable polynomial equation for describing the response surface. Several published studies have investigated the potential application of RSM to CO_2 capture processes. Serna-Guerrero *et al*. (2010) determined the influence of desorption pressure, desorption temperature, gas flow rate, and their corresponding interactions on the regeneration performance (working capacity and desorption rate) of an amine-based CO_2 adsorption process by RSM [19]. Mulgundmath and Tezel (2010) investigated the influence of four control parameters (*i.e.* purge/feed flow ratio, purge time, purge gas temperature and adsorption pressure) on CO_2 recovery in a temperature pressure swing adsorption (TPSA) system [20]. Nuchitprasittichai and Cremasch (2011) optimized the amine based CO_2 capture process by RSM [21]. The impacts of the absorber and stripper column heights, the concentration of amine solvents, and operating condition of the CO_2 recovery and energy consumption with various amine solvents was studied in detail. García *et al*. (2011) used the RSM method to investigate the influence of the adsorption CO_2 partial pressure and temperature on CO_2 capture capacity and the breakthrough time of activated carbon [22]. The combined effects of the CO_2 partial pressure and temperature on CO_2 capture capacity and breakthrough time of the adsorption process was evaluated.

The objective of this work is to optimize the cryogenic CO_2 capture efficiency of the free piston Stirling cooler (FPSC) system using RSM. The vital parameters that affect the capture performance have been identified as the flow rate of flue gas,

temperature of FPSC-1 (which is used to chill the flue gas and separate H_2O) and idle operating time before gas inflow [23]. On the other hand, CO_2 recovery, energy consumption and CO_2 productivity are representative of system performance.

The paper is organized as follows: Section 2 introduces the CO_2 capture process based on the FPSCs system. Section 3 describes the structure of the system and experiment design by RSM. Section 4 discusses the impact of parameters on CO_2 recovery, energy consumption and CO_2 productivity. Section 5 summarizes the optimum condition of the novel cryogenic CO_2 capture process.

2. Cryogenic CO_2 capture process based on FPSCs

The schematic of the cryogenic process is shown in Fig. 1. The whole process can be divided into 3 sections: 1) cryogenic unit 1 (C-1); 2) cryogenic unit 2 (C-2); 3) cryogenic unit 3 (C-3) [24].

2.1. Cryogenic unit 1 (C-1)

First, flue gas is chilled by FPSC-1 in the cryogenic unit 1 (C-1). At C-1, the moisture in the feed gas condenses into water and then flows out from the outlet to avoid clogging the vessel. This is the key issue of cryogenic CO_2 separation technologies. The dry flue gas is prechilled to a low temperature to facilitate CO_2 anti-sublimation in the subsequent stage. In order to improve the exergy efficiency of the whole process, the latent and sensible heat of the condensate water is recuperated by the heat exchanger with the incoming hot flue gas.

2.2. Cryogenic unit 2 (C-2)

In cryogenic unit 2 (C-2), FPSC-2 provides the cryogenic condition, and the flue gas is cooled down to below -100°C. According to the work of Clodic *et al*., the freezing point of CO_2 for the flue gas from a typical coal-fired power plant (typically 3 ~ 20 % CO_2) varies in the range of -112 ~ -97 °C [13]. In our research, the percentage of CO_2 in flue gases is about 13 vol%, and which consequently has a frost point of approximately -100 °C. When the gas stream passes through the low temperature cold head, the CO_2 immediately solidifies into dry ice and frosts on the surface of the cold head. In comparison, other gas (such as N_2) is exhausted without phase change. Meanwhile, the sensible heat of the cold residual gas is also recovered by the subsequent flue gas.

2.3. Cryogenic unit 3 (C-3)

In this section, a motor driven scraping rod is utilized to separate the deposited CO_2 from the surface of the cold head, and the captured CO_2 is gathered in cryogenic unit 3 (C-3), where FPSC-3 provides a low temperature condition (below -78.5 °C) to store dry ice and prevent it gasifying. In order to separate CO_2 from the residual gas, the frosted CO_2 is temporarily stored in C-3. Since the latent heat of the frosted CO_2 is substantial, its cold energy is recovered by the heat exchanger. During the CO_2 sublimation process, an amount of sensible heat is required and is absorbed from the hot gas stream. Thus, the incoming flue gas is sufficiently chilled before pumping into the cryogenic units.

3. Experimental

3.1. Apparatus

The structure of the experimental apparatus is shown in Fig. 2. The system detail has been described in previous work [25,26]. It is noteworthy that a couple of improvements in the system have been carried out. First, the tower body and its junctions have been wrapped with thermal insulation material (expand aple poly ephylene); second, the FPSC-1 was replaced by a low power unit (80 W) to save input electricity.

The composition of the flue gas from a typical coal-fired power plant is simulated by CO_2/13%, H_2O/5% and N_2/82%. The detailed condition of the gas mixture can be found in [25].

3.2. Experimental design

The capture performance based on FPSCs system was optimized by RSM packages in Design Expert 7.0.10. As a convenient statistical tool, Design Expert offers multilevel factorial screening designs, and numerical optimization can be realized by analyzing the critical factors and their interactions. The design of runs was in accordance with central composite design (CCD). Based on single factor experimental results, the three major influence factors were clarified as parameters of flow rate, temperature of FPSC-1 and idle operating time before gas inflow, and each factor was manipulated in the range of 1 ~ 3 L/min, -30 ~ -10 °C and 3 ~ 5 h, respectively.

In addition, the energy consumption (EC) of the cryogenic system per unit mass CO_2 captured is defined as follows [27]:

$$\text{Energy consumption (EC)} = \frac{UI}{\left(\frac{\nu_{in}\omega_{CO_2,in}P_{in}}{T_{in}} - \frac{\nu_{out}\omega_{CO_2,out}P_{out}}{T_{out}}\right)} \cdot \frac{nR}{M_{CO_2}} \quad (1)$$

in which U and I are voltage and current in the system, respectively. $v_{CO2,\ in}$ and $v_{CO2,\ out}$ are volume flow rates of the gas mixture at the inlet and outlet. P and T are pressure and temperature at the inlet and outlet. M_{CO2} is the molar mass of CO_2.

The CO_2 capture efficiency is defined as:

$$CO_2 \text{ recovery } (\eta) = 1 - \frac{\nu_{out}\omega_{CO_2,out}P_{out}T_{in}}{\nu_{in}\omega_{CO_2,in}P_{in}T_{out}} \quad (2)$$

where η is CO_2 capture efficiency; ν is flow rate of gas mixture and ω is percentage of CO_2 in gas mixture.

Meanwhile, the CO_2 productivity can be calculated as:

$$CO_2 \text{ productivity } (\varphi) = (\nu_{in} \cdot \omega_{CO_2,in} - \nu_{out} \cdot \omega_{CO_2,out}) \cdot \rho_{CO_2} \quad (3)$$

where φ is CO_2 productivity; ρ is density of CO_2.

The experimental conditions of CCD runs of Design Expert are presented in Table 1. As shown in Table 1, the three factors chosen for this study were designated as X_1, X_2 and X_3 categorized into three levels, coded +1, 0, -1 for high, intermediate and low value, respectively. The coded values of the process parameters were determined by the following equation:

$$X_i = \frac{x_i - x_0}{\Delta x}, \quad i = 1, 2, 3 \quad (4)$$

where X_i is the coded value, x_i is the corresponding actual value, x_0 is the actual value of the independent variable at the center point, and Δx is the step change of the variable.

The behavior of the system is explained by the following quadratic polynomial equation:

$$Y_k = \beta_0 + \sum_{i=1}^{3} \beta_i X_i + \sum_{i=1}^{3} \beta_{kii} X_i^2 + \sum_{i=0}^{2} \sum_{j=i+1}^{3} \beta_{ij} X_i X_j, \quad k = 1,2; j = 2,3 \tag{5}$$

where Y_k is the k th response function. β_0, β_i , β_{ii} and β_{ij} are the coefficients of intercept, linear, quadratic and interactive terms, respectively. X_i and X_j represent the i th and j th coded independent variables.

4. Results and discussion

4.1. Statistical analysis

The analysis of variance program (ANOVA) in Design Expert software was used for regression analysis for the obtained data to estimate the coefficient of the regression equation. The fitted polynomial equation was expressed as 3D surface and contour plots in order to visualize the relationship between the responses and experimental levels of each factor and to deduce the optimum conditions. According to the analysis of variance, the effect and regression coefficients of individual linear, quadratic and interaction terms were determined. The regression coefficients were then used to generate dimensional and contour maps from the regression models.

A total of 17 runs for optimizing the three individual parameters in the CCD were undertaken and experimental conditions according to the factorial design are shown in Table 2. Results show that the CO_2 recovery, energy consumption and CO_2 productivity varied in the range of 70.49 to 95.20 %, 0.52 to 2.13 MJ/kg $_{captured}$ CO_2 and 15.89 to 45.73 kg CO_2/h, respectively.

4.2. Results of ANOVA analysis

4.2.1. CO_2 recovery

ANOVA was undertaken to obtain the process factors and response. The statistical significance was evaluated using the F-value and P-value, and the lack-of-fit value of the model indicates non-significance as desired. The goodness of fit of the polynomial model was expressed by the determination coefficient R^2, adjusted R^2 (R^2_{adj}), and predicted R^2. From the ANOVA results of CO_2 recovery (in Table 3), the results indicate the model is significant (P-value < 0.05). The lack-of-fit (4.97) implies that the result is not significant relative to pure error. The measures of R^2, adjusted R^2 (R^2_{adj}), and predicted R^2 are close to 1, which implies an adequate model. The value of the precision ratio, 23.409 indicates adequate model discrimination.

By applying multiple regression analysis to the experimental data, the predicted model of CO_2 recovery was obtained by the following second-order polynomial functions:

$$CO_2\ recovery\ (\%) = 78.29317 - 2.05444 * X_1 + 0.094756 * X_2 + 2.56601 * X_3 - 0.036137 * X_1X_2 - 1.04564 * X_1X_3 + 0.030693 * X_2X_3 + 0.75978 * X_1^2 + 4.59801E\text{-}003 * X_2^2 + 0.090564 * X_3^2 \quad (6)$$

4.2.2. Energy consumption

The ANOVA results of energy consumption are listed in Table 4. The model results indicate the model is significant (P-value < 0.05). The lack-of-fit of 0.29 implies that the result is not significant relative to pure error. The measures of R^2, adjusted R^2 (R^2_{adj}), and predicted R^2 are close to 1, which implies an adequate model. The value of the precision ratio, 22.423 indicates adequate model discrimination.

From the discussion above, it is clear that the model of energy consumption has an adequate precision. The obtained quadratic approximating model for energy consumption is described as follows:

$$Energy\ consumption\ (\mathrm{MJ/\ kg_{captured}\ CO_2}) = 2.36438 - 2.06351 * X_1 - 0.041158 * X_2 + 0.24684 * X_3 - 1.82814E\text{-}003 * X_1X_2 - 0.021632 * X_1X_3 + 3.51065E\text{-}003 * X_2X_3 + 0.37480 * X_1^2 - 6.89216E\text{-}004 * X_2^2 + 2.14984E\text{-}003 * X_3^2 \quad (7)$$

4.2.3. CO_2 productivity

The results of ANOVA analysis for CO_2 productivity are summarized in Table 5. The results indicate the model is significant (P-value < 0.05). The lack-of-fit of 3.85 implies that the result is not significant relative to pure error. The measures of R^2, adjusted R^2 (R^2_{adj}), and predicted R^2 are close to 1, which implies an adequate model.

The value of precision ratio 20.104 indicates adequate model discrimination.

In light of the ANOVA analysis, the predicted model of CO_2 productivity can be calculated by the following second-order polynomial equation:

$$\begin{aligned} CO_2\ productivity\ (kg/h) = {} & 21.43727 + 5.18471 * X_1 + 13.91162 * X_2 - 3.17533 * X_3 \\ & - 1.86241 * X_1X_2 + 7.74237 * X_1X_3 + 0.382177 * X_2X_3 \\ & + 3.74721 * X_1^2 + 0.015271 * X_2^2 + 2.113741 * X_3^2 \end{aligned} \quad (8)$$

4.3. Model validation

In order to confirm the RSM validity, the model equation for predicting the optimum response values was tested using the selected conditions. Three confirmation experiments were implemented with process parameters chosen randomly from the ranges of Table 1 in order to validate the mathematical models. The actual results in terms of the average of three measured results were calculated. Table 6 shows the actual values, predicted values and calculated error of confirmation experiments. Fig. 3 shows respective plots of actual and predicted value of CO_2 recovery (a), energy consumption (b) and CO_2 productivity (c). The results illustrate that the developed models can effectively predict the capture performance (CO_2 recovery, energy consumption and CO_2 productivity) of the cryogenic system.

4.4. Optimization of CO_2 recovery

In this section, process optimization was implemented to find the conditions under which maximum CO_2 recovery is possible. 3D response surface and 2D contour plots indicate the effects of parameters and their interactions on CO_2 recovery. The optimal values of the selected variables were obtained by solving the regression equations.

They show the type of interactions between two tested variables and the relationship between responses and experiment levels of each variable. Two variables within the experimental range are depicted in the 3D surface plots when the third variable was kept constant at zero.

Fig. 4-6 show the results of CO_2 recovery affected by flow rate (X_1), temperature of FPSC-1 (X_2) and idle operating time (X_3). Fig. 4 shows the 3D surface plot and the contour plot of the effect of the flow rate (X_1) and temperature of FPSC-1 (X_2) on CO_2 recovery. It is clear that the CO_2 recovery increased from 74.37 to 95.23 % with an increased feed gas of 1.0 to 2.2 L/min. Then, CO_2 recovery decreases from 95.23 to 74.75 % with the flow rate varying from 2.2 to 3.0 L/min. This is because when the flow rate is lower than 2.2 L/min, the cold head can capture the majority of the CO_2 in the gas mixture. However, when the flow rate increased to higher than 2.2 L/min, the amount of CO_2 passed through the low temperature surface of the cold head without anti-sublimation process, and thus the CO_2 recovery decreased dramatically. When the temperature of FPSC-1 dropped from -10 to -18 °C, the CO_2 recovery increased from 75.57 to 95.21%. If the temperature continually decreased to -30 °C, the CO_2 recovery decreased gradually (from 95.21 to 72.11 %).

Fig. 5 shows the effect of the flow rate (X_1) and idle operating time (X_3) on CO_2 recovery. It indicates that while the idle operating time decreased from 5.0 to 3.9 h, the CO_2 recovery of the system increased from 73.45 to 95.16 %. In contrast, the idle operating time varied from 3.9 to 3.0 h, the CO_2 recovery decreased to 74.33 %. This

is because when the idle operating time is near 5 h, the system was excessively pre-chilled to solidify H_2O into ice indirectly, and the ice clogged the vessel. This would adversely affect the anti-sublimation of CO_2, and then lead to low CO_2 recovery. In comparison, when the idle operating time is too short (around 3 h), a fraction of H_2O in the flue gas could not be separated effectively and was pumped into the cryogenic unit 2 along with the gas stream. Under the low temperature condition, the H_2O solidified and frosted on the surface of the cold head, which prevents heat and mass transfer in the CO_2 anti-sublimation stage. From Fig. 5, the effect of flow rate on CO_2 recovery can also be observed. The optimal flow rate of the gas stream is around 2.1 L/min with the a CO_2 recovery of 95.16%, and this is in accordance with the result in Fig. 4.

Fig. 6 shows the effect of the temperature of FPSC-1 (X_2) and idle operating time (X_3) on CO_2 recovery. The contour plot indicates that when the temperature of FPSC-1 dropped from -10 to -17°C, CO_2 recovery increased gradually (from 79.45 to 95.08%). However, while the temperature steadily decreased to -30°C, CO_2 recovery reduced rapidly. This is because the function of FPSC-1 is to chill the cryogenic unit 1 (C-1) and condense moisture from the flue gas. When the temperature of FPSC-1 is higher than -17 °C, the moisture in the gas stream flowed into C-2 and solidified into ice on the surface of the cold head and adversely affected the anti-sublimation of the incoming CO_2 gas. While the temperature is lower than -17 °C, the flue gas cannot be effectively pre-chilled, and the CO_2 recovery is also reduced. In addition, the influence of the idle operating time on the CO_2 recovery is also depicted in Fig. 6. The

optimal idle operating time is around 4.2 h with CO_2 recovery of 94.87%.

4.5. Optimization of energy consumption

Response surfaces were plotted to study the effects of parameters and their interactions on energy consumption. The results of energy consumption affected by flow rate (X_1), temperature of FPSC-1 (X_2) and operating time (X_3) are shown in Fig. 7-9. These types of plots show effects of two factors on the response when the other factors were kept at zero.

Fig. 7 shows the effect of the flow rate (X_1) and temperature of FPSC-1 (X_2) on energy consumption. It indicates that the energy consumption decreased rapidly (from 2.41 to 0.53 MJ/kg $_{captured}$ CO_2) when the flue gas flow varied from 1.0 to 1.9 L/min. With increasing flow rate from 1.9 to 3.0 L/min, the energy consumption increased again from 0.53 to 2.86 MJ/kg $_{captured}$ CO_2. This is because when the flow rate is lower than 1.9 L/min, most of the CO_2 in the gas stream can be captured while it passes through the cooling fin of the cold head. However, when the flow rate is too fast (higher than 1.9 L/min), amount of CO_2 cannot be captured effectively and thus energy consumption increased. In addition, the energy consumption basically reduced (from 2.41 to 0.54 MJ/kg $_{captured}$ CO_2) when the temperature of FPSC-1 decreased from -10 to -18 °C. However, when the temperature continuously dropped to -30 °C, the energy consumption dramatically increased to 2.62 MJ/kg $_{captured}$ CO_2.

Fig. 8 shows the effect of flow rate (X_1) and idle operating time (X_3) on energy consumption. When the flow rate increased from 1.0 to 2.2 L/min, the energy

consumption of the system reduced gradually (from 2.25 to 0.53 MJ/kg $_{captured}$ CO_2). However, with the subsequent increase in the flow rate (from 2.2 to 3.0 L/min), the energy consumption increased from 0.53 to 1.94 MJ/kg $_{captured}$ CO_2. This is consistent with the obtained optimal flow rate shown in Fig. 7. In addition, the energy consumption can be obviously minimized (from 2.25 to 0.52 MJ/kg $_{captured}$ CO_2) when the idle operating time is shortened from 5.0 to 3.8 h. When the idle operating time continually dropped to 3.0 h, the energy consumption dramatically increased to 1.97 MJ/kg $_{captured}$ CO_2. This is because when the idle operating time decreased from 5.0 to 3.8 h, the operating cost of the system was significantly reduced while the CO_2 recovery of the system can be still kept at approximately 95 %. In contrast, when the idle operating time is too short (up to 3.0 h), the low temperature of the system cannot reach the condensing and freezing point of the corresponding components (H_2O and CO_2), and thus the energy consumption increase.

Fig. 9 illustrates the interaction of the temperature of FPSC-1 (X_2) and operating time (X_3) on energy consumption. It can be seen that the energy consumption of the system decreased gradually from 1.78 to 0.52 MJ/kg $_{captured}$ CO_2 with the temperature of FPSC-1varied from -30 to -20 °C. When the temperature continuously rose from -20 to -10 °C, the energy consumption increased from 0.52 to 1.96 MJ/kg $_{captured}$ CO_2. In contrast, the energy consumption decreased from 1.81 to 0.52 MJ/kg $_{captured}$ CO_2 with idle operating time increasing from 3.0 h to 3.8 h. When the idle operating time continuously extended from 3.8 h to 5.0 h, energy consumption increased from 0.52 to 2.1 MJ/kg $_{captured}$ CO_2. Therefore, it can be concluded that the optimal idle operating

time and temperature of FPSC-1 are 3.8 h and -20 °C.

4.6. Optimization of CO_2 productivity

Fig. 10 shows the 3D surface plot and the contour plot of the effect of the flow rate (X_1) and temperature of FPSC-1 (X_2) on CO_2 productivity. It is clear that the CO_2 productivity increased from 15.37 to 44.37 kg/h with increasing flow rate of feed gas from 1.0 to 2.0 L/min. Then, the CO_2 productivity decreases from 45.37 to 16.82 kg/h with the flow rate varying from 2.0 to 3.0 L/min. When the flow rate is lower than 2.0 L/min, the majority of the CO_2 in the gas mixture can be captured by the cold head. However, when the flow rate increased to higher than 2.0 L/min, the amount of CO_2 passed through the low temperature surface of the cold head without anti-sublimation process, and thus the CO_2 productivity decreased dramatically. When the temperature of FPSC-1 dropped from -10 to -21 °C, the CO_2 productivity of the process increased from 16.01 to 44.53 kg/h. Therefore, if the temperature continually decreased to -30 °C, the CO_2 productivity decreased gradually (from 44.53 to 16.84 kg/h).

Fig. 11 shows the effect of the flow rate (X_1) and idle operating time (X_3) on CO_2 productivity. It indicates that while the idle operating time decreased from 5.0 to 4.2 h, the CO_2 productivity of the system increased from 15.79 to 45.21 kg/h. In contrast, when the idle operating time varied from 4.2 to 3.0 h, the CO_2 productivity decreased to 17.12 kg/h. The influence of idle operating time indicates that when the idle operating time is near 5 h, the system was excessively pre-chilled to solidify H_2O into ice indirectly, and ice clogged the vessel. This would adversely affect the

anti-sublimation of CO_2, and lead to low CO_2 productivity. In comparison, when the idle operating time is too short (around 3 h), a fraction of H_2O in the flue gas could not be separated effectively and was pumped into the cryogenic unit 2 along with the gas stream. Under low temperature conditions, the H_2O solidified and frosted on the surface of the cold head which prevents heat and mass transfer in the CO_2 anti-sublimation stage. In addition, the effect of flow rate on the CO_2 productivity can be observed. It was noted that the optimal flow rate of the gas stream is around 2.2 L/min with the CO_2 productivity of 44.97 kg/h,.

Fig. 12 shows the effect of the temperature of FPSC-1 (X_2) and idle operating time (X_3) on CO_2 productivity. The contour plot indicates that when the temperature of FPSC-1 dropped from -10 to -19 °C, CO_2 productivity increased gradually (from 16.22 to 44.17 kg/h). However, when the temperature continually decreased to -30 °C, CO_2 productivity reduced rapidly. This is because the function of FPSC-1 is to chill the cryogenic unit 1 (C-1) and condense moisture from the flue gas. When the temperature of FPSC-1 is higher than -19 °C, the moisture in the gas stream flowed into C-2 and solidified into ice on the surface of the cold head and adversely affected the anti-sublimation of the incoming CO_2 gas. When the temperature is lower than -19 °C, the flue gas cannot be effectively pre-chilled, and CO_2 productivity also reduces. In addition, the influence of the idle operating time on the CO_2 productivity is depicted in Fig. 12. The optimal idle operating time is around 4.0 h with CO_2 productivity of 44.34 kg/h.

4.7. Prospective for scaling up of the system

In order to commercially apply the developed system for the industrial emissions, investigation of the feasibility of scaling up the developed cryogenic CO_2 capture process is significant. To process the enormous flow of flue gas in a scaled up plant, the following measures should be carried out: 1) the diameter of separation tower must be correspondingly increased. 2) The number of Stirling coolers in different stages (pre-freezing, main freezing and storage) should also be increased. 3) From the current situation, heat loss would be an unavoidable challenge due to the huge temperature difference between the internal and external features of the installation and can be overcome by an effective heat recovery process.

5. Conclusion

The optimization of the cryogenic CO_2 capture process based on the FPSCs system was analyzed focusing on CO_2 recovery and energy consumption. The optimization employed an RSM experimental design to obtain operational conditions for maximum CO_2 recovery and minimum energy consumption. The optimization results show that the flow rate of feed gas (X_1), temperature of FPSC-1 (X_2) and idle operating time (X_3) of the system have a significant effect on CO_2 recovery and energy consumption. The optimal condition of the system is as follows: flow rate of flue gas is 2.16 L/min, temperature of FPSC-1 is -18 $^{\circ}$C and idle operating time is 3.9 h. Under these conditions, 95.20 % CO_2 can be removed from flue gas and energy consumption is 0.52 MJ/kg $_{\text{captured}}$ CO_2. Meanwhile, the CO_2 productivity is 44.37 kg CO_2/h.

It is worth noting that for the RSM approach, the stated value of the independent variables must fall within the prescribed limits. When the value of each factor is beyond the boundary, the developed model will become invalid. In future, a more effective approach (such as a neural network method) should be considered to avoid this disadvantage.

Acknowledgements

We thank Mr. Yamano and Mr. Yamasaki in Tanabe Engineering Corporation for their technical assistance.

References

[1] Aaron D, Tsouris C. Separation of CO_2 from flue gas: a review. Sep Sci Technol 2005;40: 321-48.

[2] Inventory of U.S. Greenhouse Gas Emissions and Sinks, 2008. EPA.

[3] Houghton J. Global warming. Rep Prog Phys 2005;68(6):1343-403.

[4] Wang M, Lawal A, Stephenson P, Sidders J, Ramshaw C. Post-combustion CO_2 capture with chemical absorption: A state-of-the-art review. Chem Eng Res Des 2011; 89:1609-24.

[5] Huang CC, Shen SC. Adsorption of CO_2 on chitosan modified CMK-3 at ambient temperature. J Taiwan Inst Chem Eng 2013;44:89-94

[6] Kuramochi T, Ramírez A, Turkenburg W, Faaij A. Comparative assessment of CO_2 capture technologies for carbon-intensive industrial processes. Prog Energ Combust. 2012;38:87-112.

[7] Rubin ES, Mantripragada H, Mark A, Versteeg P, Kitchin J. The outlook for improved carbon capture technology. Prog Energ Combust 2012;38:630-71.

[8] Li CC, Cheng JY, Liu WH, Huang CM, Hsu HW, Lin HP. Enhancement in cyclic stability of the CO_2 adsorption capacity of CaO-based sorbents by hydration for the calcium looping cycle. J Taiwan Inst Chem Eng (2013), http://dx.doi.org/10.1016/j.jtice.2013.06.019.

[9] Clausse M, Merel J, Meunier F. Numerical parametric study on CO_2 capture by indirect thermal swing adsorption. Int J Greenhouse Gas Control 2011;5:1206-13.

[10] Li H, Yan J, Campana PE. Feasibility of integrating solar energy into a power plant with amine-based chemical absorption for CO_2 capture. Int J Greenhouse Gas Control 2012;9:272-80.

[11] Holmes AS, Ryan JM. Cryogenic distillative separation of acid gases from methane. US Patent 1982;4,318,723.

[12] Thomas ER, Denton RD. Conceptual Studies for CO_2/Natural Gas Separation Using the Controlled Freeze Zone (CFZ) Process, Gas Sep Purif 1988;2:84-9.

[13] Clodic D, Younes M. A new method for CO_2 capture: frosting CO_2 at atmospheric pressure. In: Sixth International Conference on Greenhouse Gas Control Technologies, GHGT6, Kyoto, October 2002, p. 155-60.

[14] Tuinier MJ, Annaland MS, Kramer GJ, Kuipers JAM. Cryogenic CO_2 capture using dynamically operated packed bed. Chem Eng Sci 2010;65:114-9.

[15] Tuinier MJ, van Sint Annaland M. Biogas purification using cryogenic packed-bed technology. Ind Eng Chem Res 2012;51:5552-8.

[16] Berstad D, Nekså P, Anantharaman R. Low-temperature CO_2 removal from natural gas.

Energy Procedia 2012;26:41-8.

[17] Song CF, Kitamura Y, Li SH, Jiang WZ. Analysis of CO_2 frost formation properties in cryogenic capture process. Int J Greenhouse Gas Control 2013;13:26-33.

[18] Myers RH, Montgomery DH. Response Surface Methodology. John Wiley & Sons, USA. 1995.

[19] Serna-Guerrero R, Belmabkhout Y, Sayari A. Influence of regeneration conditions on the cyclic performance of amine-grafted mesoporous silica for CO_2 capture: An experimental and statistical study. Chem Eng Sci 2010;65:4166-72.

[20] Mulgundmath V, Tezel F. Optimisation of carbon dioxide recovery from flue gas in a TPSA system. Adsorption 2010;16:587-98.

[21] Nuchitprasittichai A, Cremaschi S. Optimization of CO_2 capture process with aqueous amines using response surface methodology. Comput Chem Eng 2011;35:1521-31.

[22] García S, Gil MV, Martín CF, Pis JJ, Rubiera F, Pevida C. Breakthrough adsorption study of a commercial activated carbon for pre-combustion CO_2 capture. Chem Eng J 2011;171:549- 56.

[23] Song CF, Kitamura Y, Li SH. Evaluation of Stirling cooler system for cryogenic CO_2 capture. Appl Energy 2012;98:491-501.

[24] Song C, Kitamura Y, Li S, Lu J. Deposition CO_2 Capture Process Using a Free Piston Stirling Cooler. Ind Eng Chem Res 2013;52 (42):14936-43.

[25] Song CF, Kitamura Y, Li SH, Jiang WZ. Parametric analysis of a novel cryogenic CO_2 capture system based on Stirling coolers. Environ Sci Technol 2012;46:12735-41.

[26] Song CF, Kitamura Y, Li SH, Ogasawara KJ. Design of a cryogenic CO_2 capture system based on Stirling coolers. Int J Greenhouse Gas Control 2012;7:107-14.

[27] Song C, Kitamura Y, Li S. Energy analysis of the cryogenic CO_2 capture process based on Stirling coolers. Energy doi:10.1016/j.energy.2013.10.087.

Figure captions

Fig. 1 Schematic of cryogenic capture process

Fig. 2 The structure of the exploited cryogenic CO_2 capture system

Fig. 3 Relationship between experimental and predicted values. (a) CO_2 recovery (%), (b) energy consumption (MJ/kg $_{captured}$ CO_2) and (c) CO_2 productivity (kg/h)

Fig. 4 Interaction effect of flow rate (X_1) and temperature of FPSC-1 (X_2) on CO_2 recovery (%). (a) 3D surface plot; (b) contour plot.

Fig. 5 Interaction effect of flow rate (X_1) and operating time (X_3) on CO_2 recovery (%). (a) 3D surface plot; (b) contour plot.

Fig. 6 Interaction effect of temperature of FPSC-1 (X_2) and operating time (X_3) on CO_2 recovery (%). (a) 3D surface plot; (b) contour plot.

Fig. 7 Interaction effect of flow rate (X_1) and temperature of FPSC-1 (X_2) on energy consumption (MJ/kg $_{captured}$ CO_2). (a) 3D surface plot; (b) contour plot.

Fig. 8 Interaction effect of flow rate (X_1) and operating time (X_3) on energy consumption (MJ/kg $_{captured}$ CO_2). (a) 3D surface plot; (b) contour plot.

Fig. 9 Interaction effect of temperature of FPSC-1 (X_2) and operating time (X_3) on energy consumption (MJ/kg $_{captured}$ CO_2). (a) 3D surface plot; (b) contour plot.

Fig. 10 Interaction effect of flow rate (X_1) and temperature of FPSC-1 (X_2) on CO_2 productivity (kg/h). (a) 3D surface plot; (b) contour plot.

Fig. 11 Interaction effect of flow rate (X_1) and operating time (X_3) on CO_2 productivity (kg/h). (a) 3D surface plot; (b) contour plot.

Fig. 12 Interaction effect of temperature of FPSC-1 (X_2) and operating time (X_3) on CO_2 productivity (kg/h). (a) 3D surface plot; (b) contour plot.

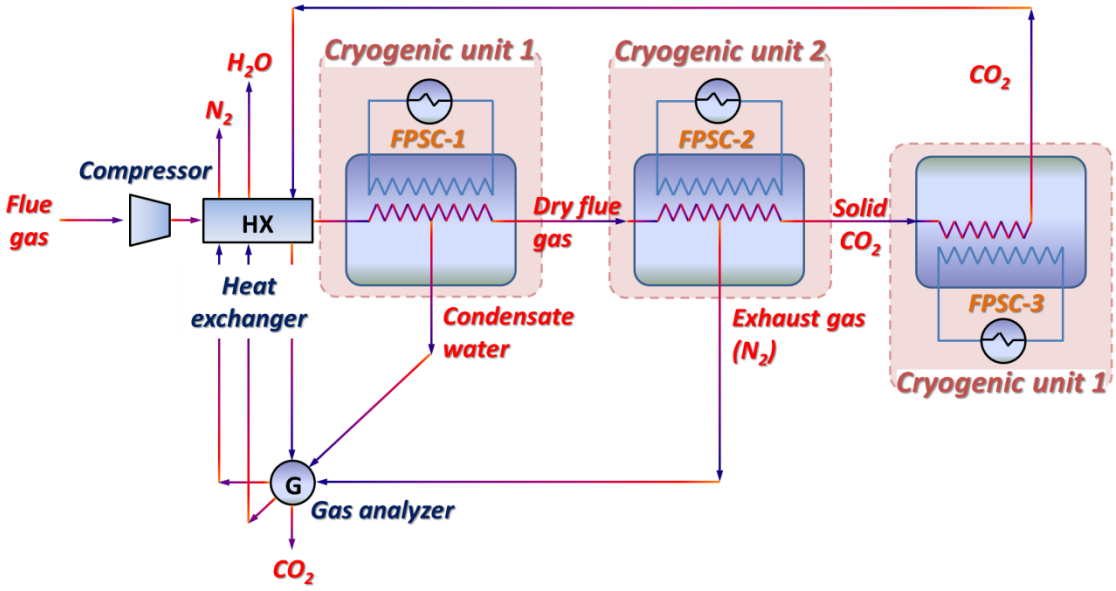

Fig. 1 Schematic of cryogenic capture process

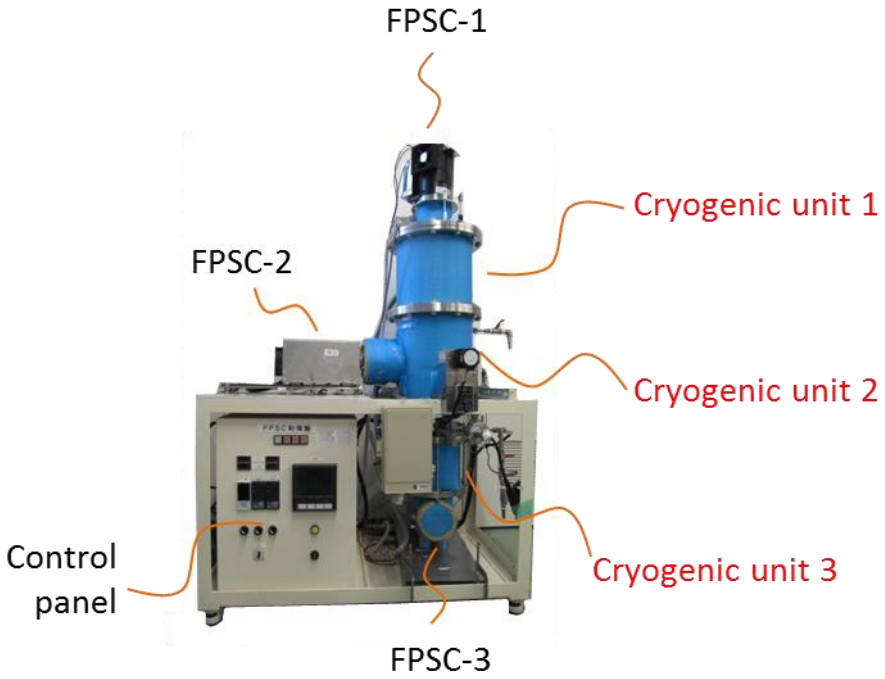

Fig. 2 The structure of the exploited cryogenic CO_2 capture system

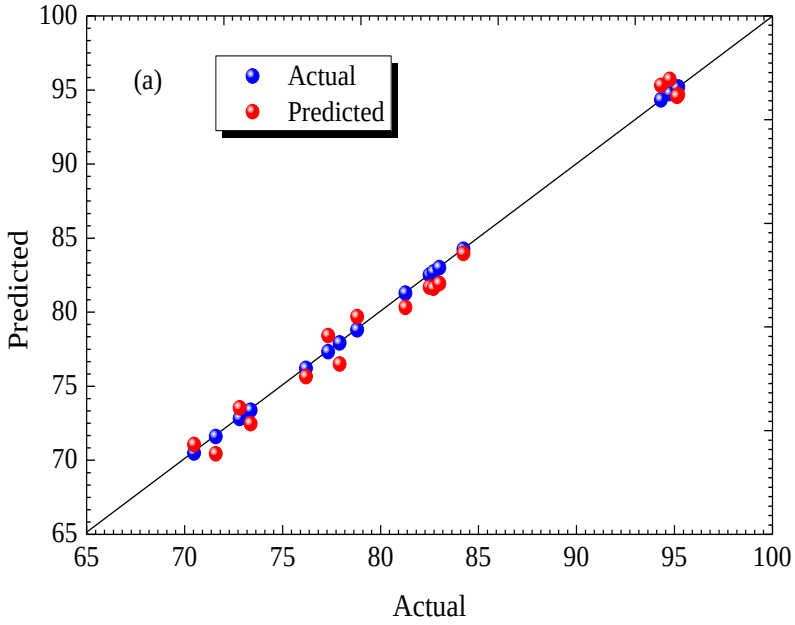
(a)
Actual
Predicted
Predicted
Actual
100
95
90
85
80
75
70
65
65
70
75
80
85
90
95
100

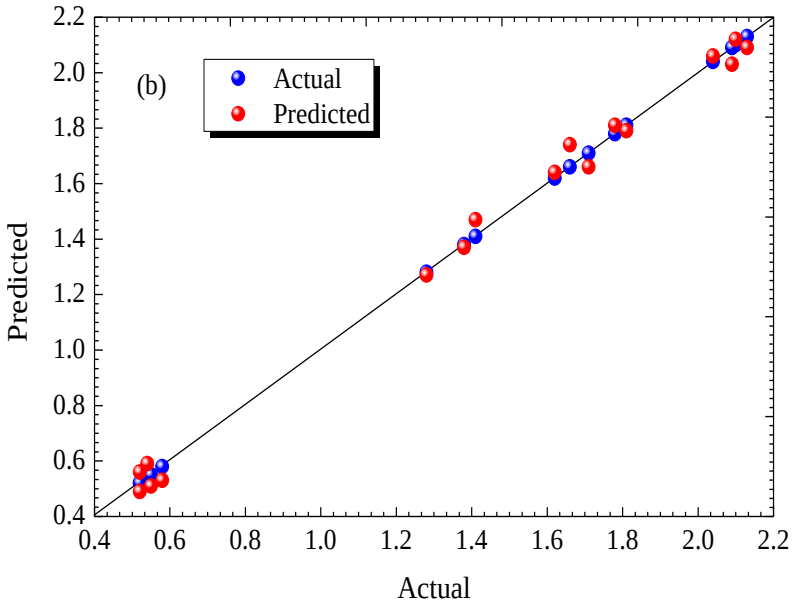
(b)
Actual
Predicted
Predicted
Actual
2.2
2.0
1.8
1.6
1.4
1.2
1.0
0.8
0.6
0.4
0.4
0.6
0.8
1.0
1.2
1.4
1.6
1.8
2.0
2.2

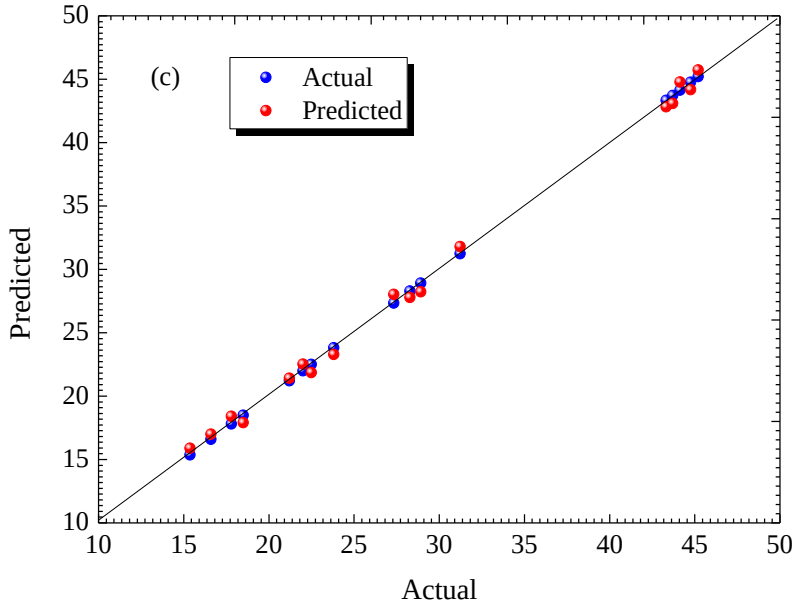

Fig. 3 Relationship between experimental and predicted values. (a) CO_2 recovery (%), (b) energy consumption ($MJ/kg_{captured}$ CO_2) and (c) CO_2 productivity (kg/h)

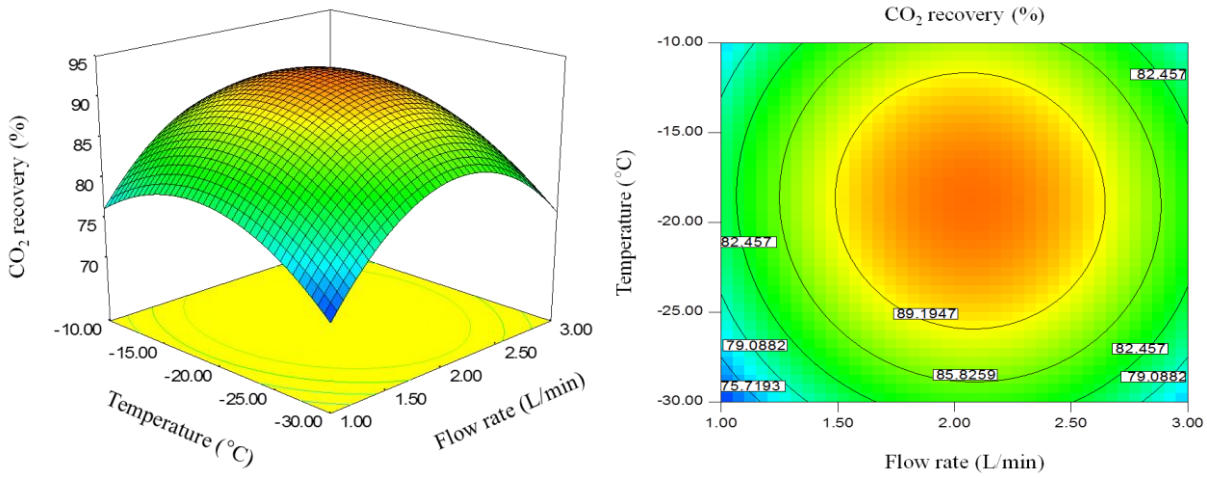

(a) (b)

Fig. 4 Interaction effect of flow rate (X_1) and temperature of FPSC-1 (X_2) on CO_2 recovery (%). (a) 3D surface plot; (b) contour plot

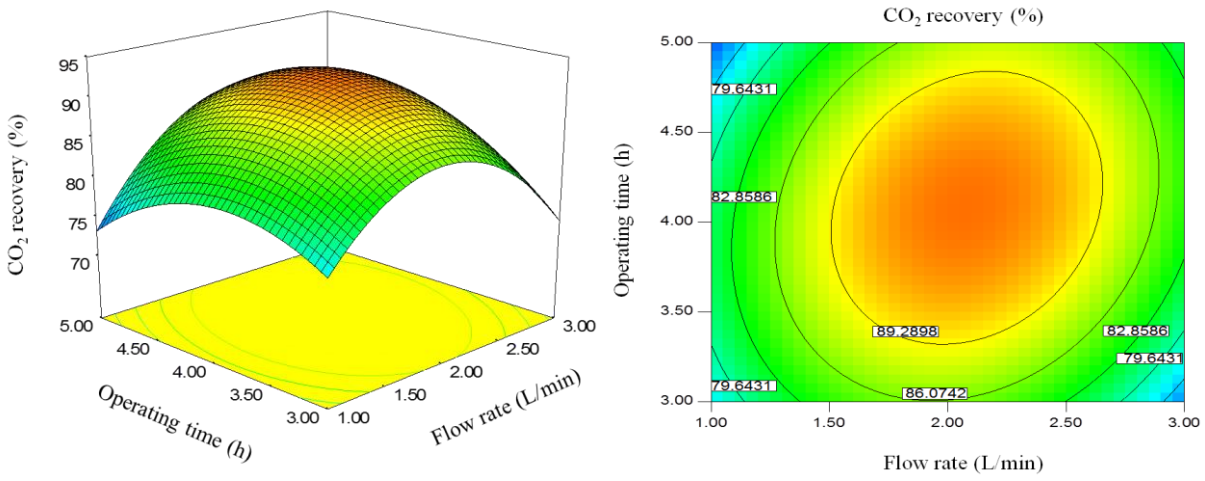

(a) (b)

Fig. 5 Interaction effect of flow rate (X_1) and operating time (X_3) on CO_2 recovery (%). (a) 3D surface plot; (b) contour plot

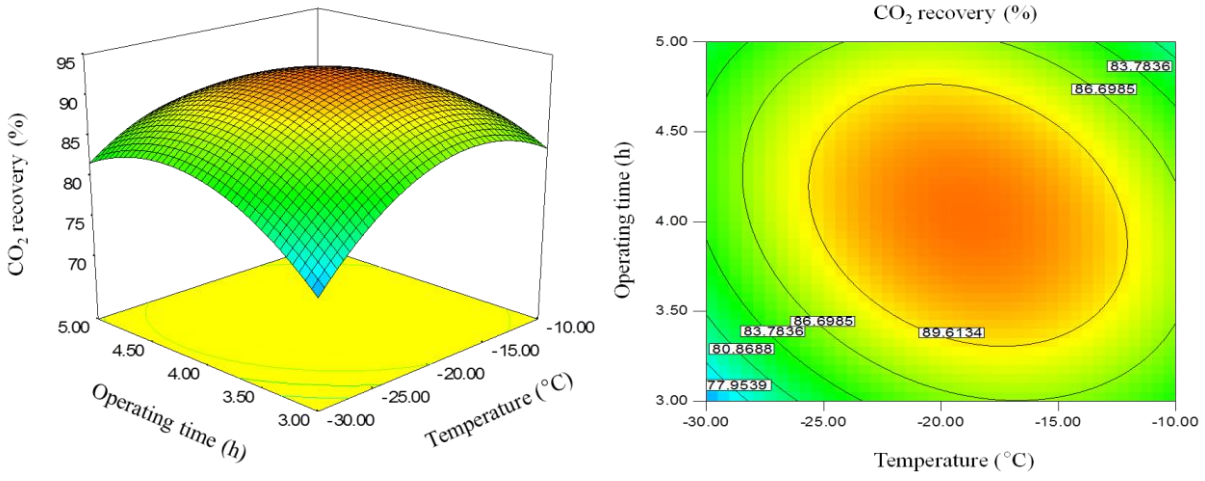

(a) (b)

Fig. 6 Interaction effect of temperature of FPSC-1 (X_2) and operating time (X_3) on CO_2 recovery (%). (a) 3D surface plot; (b) contour plot

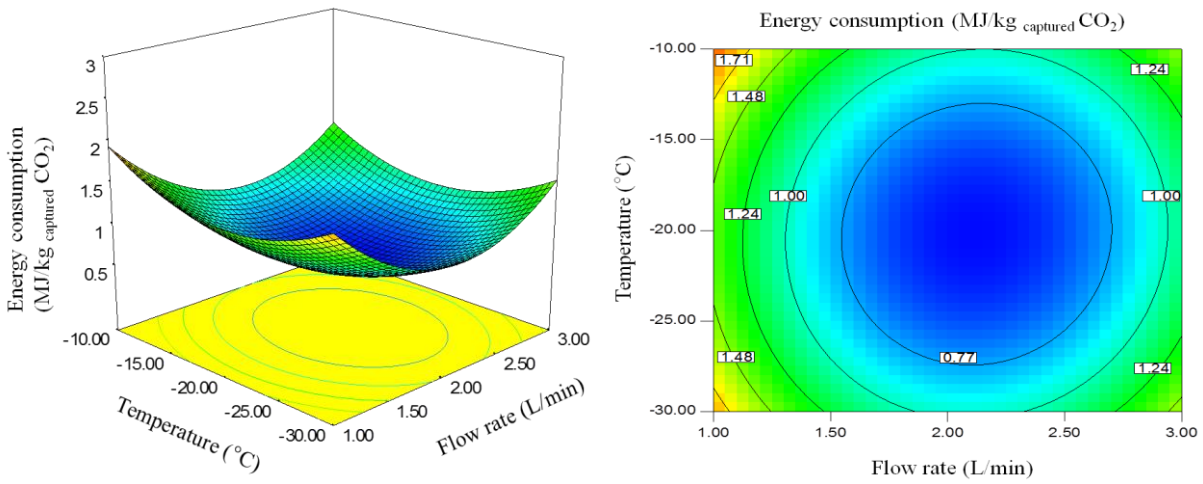

(a) (b)

Fig. 7 Interaction effect of flow rate (X_1) and temperature of FPSC-1 (X_2) on energy consumption (MJ/kg $_{captured}$ CO_2).

(a) 3D surface plot; (b) contour plot

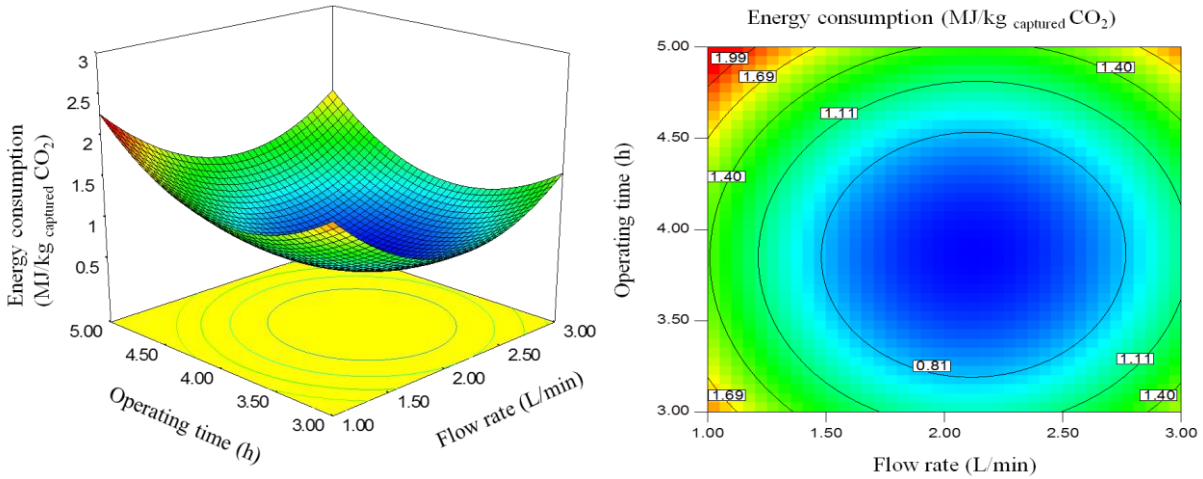

(a) (b)

Fig. 8 Interaction effect of flow rate (X_1) and operating time (X_3) on energy consumption (MJ/kg $_{captured}$ CO_2). (a) 3D surface plot; (b) contour plot

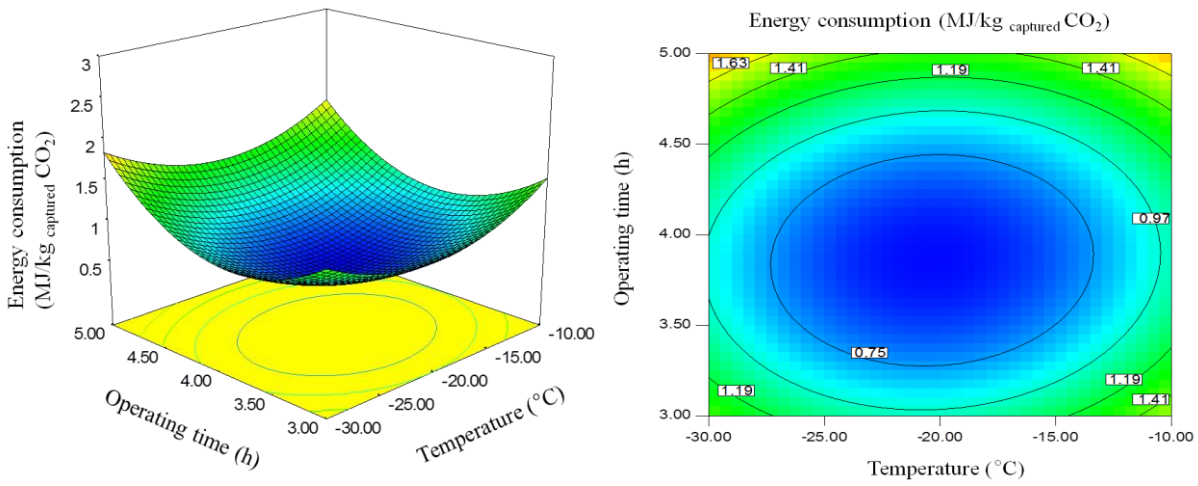

(a) (b)

Fig. 9 Interaction effect of temperature of FPSC-1 (X_2) and operating time (X_3) on energy consumption (MJ/kg $_{captured}$ CO_2). (a) 3D surface plot; (b) contour plot

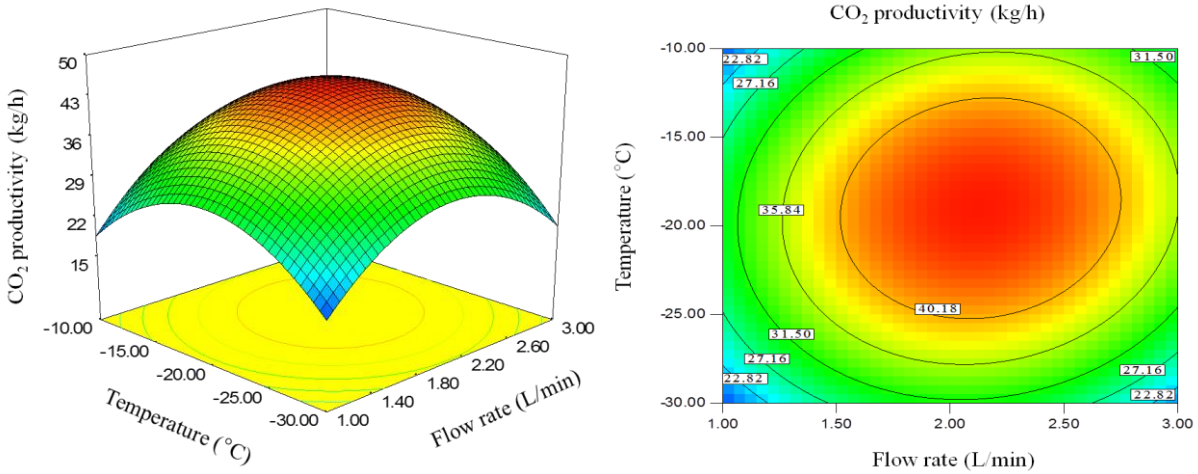

(a) (b)

Fig. 10 Interaction effect of flow rate (X_1) and temperature of FPSC-1 (X_2) on CO_2 productivity (kg/h). (a) 3D surface plot; (b) contour plot

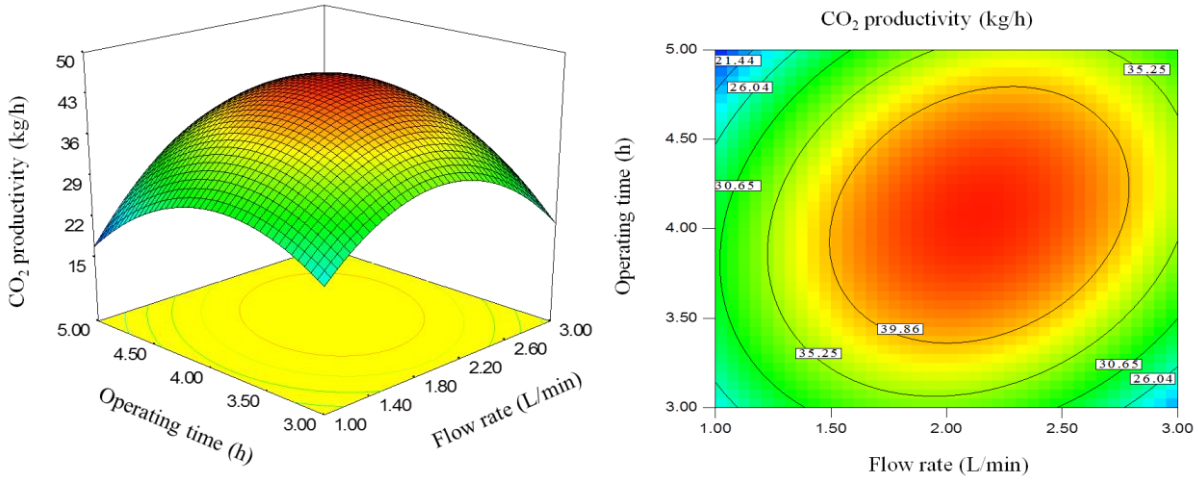

(a) (b)

Fig. 11 Interaction effect of flow rate (X_1) and operating time (X_3) on CO_2 productivity (kg/h). (a) 3D surface plot; (b) contour plot

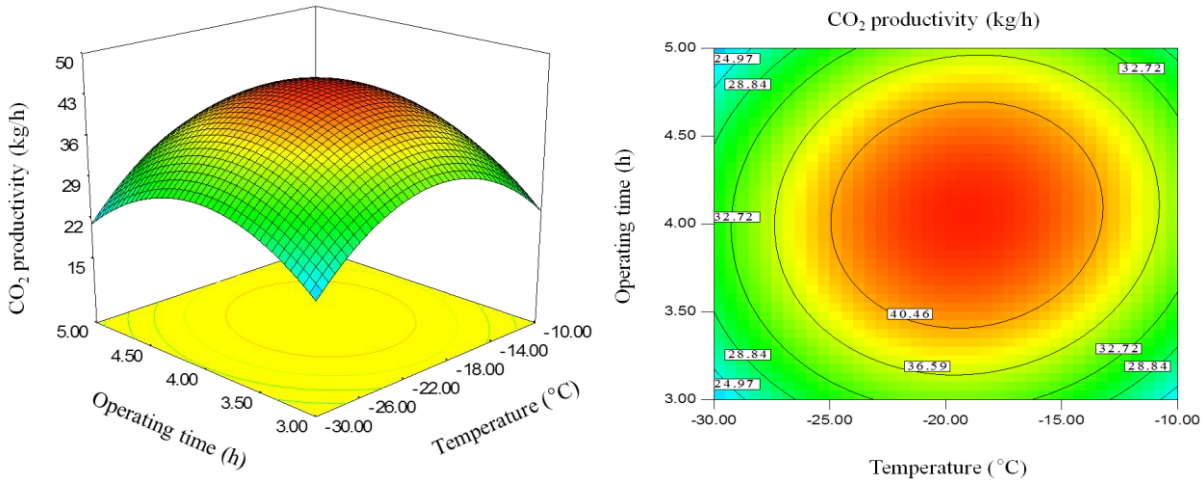

(a) (b)

Fig. 12 Interaction effect of temperature of FPSC-1 (X_2) and operating time (X_3) on CO_2 productivity (kg/h). (a) 3D surface plot; (b) contour plot

Table captions

Table 1 Independent variables and their levels.

Table 2 Experimental matrix for CCD during the capture process.

Table 3 ANOVA analysis for CO_2 recovery (η) model.

Table 4 ANOVA analysis for energy consumption (EC) model.

Table 5 ANOVA analysis for CO_2 productivity (φ) model.

Table 6 Results of validation test.

Table 1

Independent variables and their levels.

Factors	Tag	Symbol	Units	level		
				-1	0	1
Flow rate of flue gas	v	X_1	L/min	1	2	3
Temperature of FPSC-1	T	X_2	℃	-30	-20	-10
Idle operating time	t	X_3	h	3	4	5

Table 2

Experimental matrix for CCD during the capture process.

Run no.	Experimental information						Results					
	X_1 (ν-L/min)		X_2 (T-°C)		X_3 (t-h)		Y_1 (η-%)		Y_2 (EC-MJ/kg $_{captured}$ CO_2)		Y_3 (φ-kg/ h)	
	Coded	Actual	Coded	Actual	Coded	Actual	Experimental	Predicted	Experimental	Predicted	Experimental	Predicted
1	0	2	-1	-30	-1	3	70.49	71.06	1.38	1.37	18.49	17.89
2	1	3	0	-20	-1	3	76.20	75.64	1.71	1.66	21.20	21.40
3	-1	1	0	-20	-1	3	81.28	80.32	1.66	1.74	28.29	27.79
4	-1	1	0	-20	1	5	71.60	70.44	2.13	2.09	16.60	16.99
5	0	2	0	-20	0	4	94.32	95.31	0.54	0.56	43.33	42.83
6	0	2	0	-20	0	4	95.20	94.67	0.52	0.53	45.20	45.73
7	0	2	0	-20	0	4	94.76	95.71	0.55	0.51	44.76	44.18
8	0	2	1	-10	-1	3	82.50	81.68	1.62	1.64	22.50	21.86
9	1	3	1	-10	0	4	77.92	76.5	1.28	1.27	28.92	28.22
10	0	2	0	-20	0	4	82.70	81.61	0.58	0.53	43.70	43.09
11	-1	1	-1	-30	0	4	72.81	73.53	2.04	2.06	17.81	18.41
12	1	3	0	-20	1	5	77.33	78.42	2.10	2.12	27.33	28.02
13	1	3	-1	-30	0	4	78.81	79.69	1.41	1.47	23.81	23.30
14	-1	1	1	-10	0	4	73.37	72.47	2.09	2.03	15.37	15.89
15	0	2	1	-10	1	5	84.23	83.96	1.81	1.79	31.23	31.80
16	0	2	-1	-30	1	5	83.00	81.92	1.78	1.81	22.00	22.52
17	0	2	0	-20	0	4	95.13	94.57	0.52	0.53	44.13	44.77

Table 3

ANOVA analysis for CO_2 recovery (η) model.

Factors	Sum of squares	df	Mean of squares	F-value	P-value	Significance
Model	61.81	9	6.87	44.65	<0.0001	significant
X_1	49.01	1	49.01	318.63	<0.0001	
X_2	1.20	1	1.20	7.78	0.0270	
X_3	2.74	1	2.74	17.82	0.0039	
X_1^2	2.43	1	2.43	15.80	0.0054	
X_2^2	0.89	1	0.89	5.79	0.0471	
X_3^2	0.035	1	0.035	0.22	0.6500	
X_1X_2	0.52	1	0.52	3.40	0.1079	
X_1X_3	4.37	1	4.37	28.43	0.0011	
X_2X_3	0.38	1	0.38	2.45	0.1615	
Residual	1.08	7	0.15			
Lack of Fit	0.85	3	0.28	4.97	0.0777	not significant
Pure Error	0.23	4	0.057			
Cor Total	62.89	16				

Standard deviation = 0.39	R^2 = 0.9829
Mean = 80.12	Adj R^2 = 0.9609
Coefficient of variation = 0.49	Pred R^2 = 0.7784
Predicted residual error of sum of squares = 13.94	Adeq Precision = 23.409

Table 4

ANOVA analysis for energy consumption (EC) model.

Factors	Sum of squares	df	Mean of squares	F-value	P-value	Significance
Model	3.82	9	0.42	53.64	<0.001	significant
X_1	3.02	1	3.02	381.54	<0.0001	
X_2	8.210E-003	1	8.210E-003	1.04	0.3423	
X_3	0.18	1	0.18	22.92	0.0020	
X_1^2	0.59	1	0.59	74.76	0.6933	
X_2^2	0.020	1	0.020	2.53	0.6415	
X_3^2	1.946E-005	1	1.946E-005	2.460E-003	0.4558	
X_1X_2	1.337E-003	1	1.337E-003	0.17	<0.0001	
X_1X_3	1.872E-003	1	1.872E-003	0.24	0.1559	
X_2X_3	4.930E-003	1	4.930E-003	0.62	0.9618	
Residual	0.055	7	7.912E-003			
Lack of Fit	9.864E-003	3	3.288E-003	0.29	0.8322	not significant
Pure Error	0.046	4	0.011			
Cor Total	5.86	19				

Standard deviation = 0.089	R^2 = 0.9857
Mean = 1.07	Adj R^2 = 0.9673
Coefficient of variation = 8.31	Pred R^2 = 0.9409
Predicted residual error of sum of squares = 0.23	Adeq Precision = 22.423

Table 5

ANOVA analysis for CO_2 productivity (φ) model.

Factors	Sum of squares	df	Mean of squares	F-value	P-value	Significance
Model	36.34	9	6.04	16.33	<0.001	significant
X_1	7.27	1	7.27	21.39	<0.0001	
X_2	31.63	1	31.63	237.53	0.1556	
X_3	5.58	1	5.58	0.45	0.5252	
X_1^2	5.45	1	5.45	24.39	0.0003	
X_2^2	5.28	1	5.28	24.85	0.0003	
X_3^2	3.71	1	3.71	9.75	0.0010	
X_1X_2	1.427	1	1.427	3.14	0.3207	
X_1X_3	7.937	1	7.937	29.35	0.0398	
X_2X_3	6.83	1	6.83	0.55	0.4836	
Residual	1.87	7	0.13			
Lack of Fit	0.61	3	0.18	3.85	0.0513	not significant
Pure Error	0.32	4	0.058			
Cor Total	29.24	16				

Standard deviation = 0.35	R^2 = 0.9545
Mean = 29.10	Adj R^2 = 0.8961
Coefficient of variation = 12.15	Pred R^2 = 0.7902
Predicted residual error of sum of squares = 36.55	Adeq Precision = 20.104

Table 6

Results of validation test.

Run no.	X_1 (ν-L/min)	X_2 (T-°C)	X_3 (t-h)		Y_1 (η-%)	Y_2 (EC-MJ/kg $_{captured}$ CO_2)	Y_3 (φ-kg/h)
1	1.5	-15	3.5	Experimental	81.14	1.23	21.83
				Predicted	80.34	1.21	21.45
				Error (%)	0.99	1.62	1.74
2	2.0	-20	4.0	Experimental	95.45	0.56	44.17
				Predicted	94.81	0.52	43.22
				Error (%)	1.33	3.92	2.15
3	2.5	-25	4.5	Experimental	78.09	1.48	33.94
				Predicted	78.83	1.51	33.51
				Error (%)	0.95	2.03	1.27